SEMICONDUCTOR LASER BASED TRACE GAS SENSOR TECHNOLOGY: RECENT ADVANCES AND APPLICATIONS

Laser Based Trace Gas Sensor Technology

FRANK K. TITTEL*, GERARD WYSOCKI, ANATOLIY KOSTEREV, YURY BAKHIRKIN
Rice University, 6100 Main Street, Electrical and Computer Engineering Department – MS 366, Houston, TX, 77005, USA

Abstract. Recent advances in the development of sensors based on infrared diode and quantum cascade lasers for the detection of trace gas species is reported. Several examples of applications in environmental and industrial process monitoring as well as in medical diagnostics using quartz enhanced photoacoustic spectroscopy and laser absorption spectroscopy will be described.

Keywords: Trace gas detection, near infrared diode lasers, mid infrared quantum and interband cascade lasers, quartz enhanced photoacoustic spectroscopy, laser absorption spectroscopy.

1. Introduction

Infrared laser absorption spectroscopy is an extremely effective tool for the detection and quantification of molecular trace gases. The demonstrated sensitivity of this technique ranges from parts per million by volume (ppmv) to the parts per trillion (pptv) level depending on the specific gas species and the detection method employed [1,2]. The spectral region of fundamental vibrational molecular absorption bands from 3 to 24 μm is the most suitable for high sensitivity trace gas detection. However the usefulness of the laser spectroscopy in this region has been limited by the availability of convenient tunable laser sources. Real world applications (see Table 1) require the laser source to be compact, efficient, reliable and operating at near room-temperatures. Existing options include lead salt diode lasers, coherent sources based on difference frequency generation (DFG) described in Part IV-2, optical parametric oscillators (see Parts II-8 and IV-3), tunable solid state lasers (see Part II-5), quantum and interband cascade lasers. Sensors based upon lead salt diode lasers are typically large in size and require

* fkt@rice.edu

M. Ebrahim-Zadeh and I.T. Sorokina (eds.), Mid-Infrared Coherent Sources and Applications, 467–493.

TABLE 1. Wide Range of Gas Sensing Applications.

Urban and Industrial Emission Measurements
Industrial Plants
Combustion Sources and Processes (e.g. early fire detection)
Automobile and Aircraft Emissions
Rural Emission Measurements
Agriculture and Animal Facilities
Environmental Gas Monitoring
Atmospheric Chemistry (e.g. ecosystems and airborne)
Volcanic Emissions
Chemical Analysis and Industrial Process Control
Chemical, Pharmaceutical, Food & Semiconductor Industry
Toxic Industrial Chemical Detection
Spacecraft and Planetary Surface Monitoring
Crew Health Maintenance & Advanced Human Life Support Technology
Biomedical and Clinical Diagnostics (e.g. breath analysis)
Forensic Science and Security
Fundamental Science and Photochemistry

cryogenic cooling because these lasers operate at temperatures of <90 K. DFG sources (especially bulk and waveguide PPLN based) have been shown recently to be robust and compact [3–5].

The recent advances of quantum cascade (QC) and interband cascade (IC) lasers fabricated by band structure engineering offer an attractive new source option for mid-infrared laser absorption spectroscopy with ultra-high resolution and sensitivity [6]. The most technologically developed mid-infrared QC laser source to date is based on type-I intersubband transitions in InGaAs/InAlAs heterostructures [7–13, Part II-1]. More recently interband cascade lasers (ICLs) based on type-II interband transition have been reported in the 3–5 μm region [14–17]. Other QCLs based on GaAs/AlGaAs material system have been reported as well [18, 19].

The vast majority of chemical substances have vibrational fundamental bands in the 3 to 24 μm region, and the absorption of light by rotational-vibrational transitions of these bands provides a nearly universal means for their sensitive and selective detection. Furthermore, near infrared spectroscopy from 1.3 to 3 μm can be used effectively in the quantification of numerous trace gas species. This application can use ultra-reliable, room temperature, single frequency distributed

feedback (DFB) lasers that were primarily developed for optical communications with output powers of up to tens of mW. These lasers access molecular overtone or combination band transitions that are typically a factor of 30 to 300 weaker than the mid-infrared fundamental transitions. However insome cases this can be compensated by the judicious choice of appropriate photoconductive or photovoltaic detectors.

Pulsed and continuous wave (cw) DFB-QC lasers allow the realization of compact, narrow linewidth sources combining single-frequency operation and substantially high powers (tens to hundreds of mWs) at mid-infrared wavelengths (3.6 to 24 μm) and temperatures attainable with thermoelectric cooling. The large wavelength coverage available with QC lasers allows identification, detection, quantification and monitoring of numerous molecular trace gas species, especially those with resolved rotational-vibrational spectra. The high QC laser output power permits the use of advanced detection techniques that significantly improve the detection sensitivity of trace gas species and decrease the complexity and size of the overall trace gas sensor architecture. This includes photoacoustic, laser absorption and cavity enhanced spectroscopy. For example, in Cavity Ringdown Spectroscopy (CRDS) [20] and Integrated Cavity Output Spectroscopy (ICOS) an effective absorption pathlength of hundreds of meters can be obtained in a compact device [21].

Unipolar DFB-QC lasers are capable of operating at high temperature of the active region. However, the power dissipation in these devices is higher than in bipolar diode lasers and can surpass 10 W. Until 2004, it was not possible to realize cw operation of QC lasers without cryogenic cooling. For example, a cw DFB-QC laser operated at 82° K in a liquid nitrogen Dewar was used in an airborne sensor for atmospheric detection of CH_4 and N_2O [22]. The cw QC-DFB laser linewidth is <1 MHz when a ripple-free current source is used [23] and can be a few 100's Hz when frequency stabilization feedback is employed [24].

An effective practical solution for non-cryogenic DFB-QC and IC laser based spectroscopy is to apply very short (5–50 ns) pump current pulses at a low duty cycle, typically $<1\%$. In pulsed operation the minimum DFB-QC laser linewidth is typically $\sim$150–350 MHz due to the frequency chirp produced by the fast heating of the active area during the pump current pulse [25]. Trace gas concentration measurements are usually performed either at pressures of $\sim$100 Torr or at atmospheric pressure (pressure broadened absorption lines are $\sim$3 GHz). Hence the pulsed mode of DFB-QC laser operation has an advantage for compact field deployable sensors because it eliminates the need for cryogenic cooling. However, recent progress in the development of cw thermoelectrically cooled Fabry-Perot and DFB QC lasers [26, 27] significantly facilitates the design of chemical sensors based on QCL technology. In addition, thermoelectrically cooled Fabry-Perot QC lasers have been used in widely tunable grating coupled cavity configurations [28–31].

2. Trace gas detection based on photoacoustic spectroscopy using QC and IC lasers

Photoacoustic spectroscopy (PAS), based on the photoacoustic effect, in which acoustic waves result from the absorption of laser radiation by a selected target compound in a specially designed cell is an effective method for sensitive trace gas detection. In contrast to other infrared absorption techniques, PAS is an indirect technique in which the effect on the absorbing medium and not the direct light absorption is detected. Light absorption results in a transient temperature effect, which then translates into pressure variations in the absorbing medium that can be detected with a sensitive microphone. PAS is ideally a background-free technique, since the signal is generated only by the absorbing gas. However, background signals can originate from nonselective absorption of the gas cell windows (coherent noise) and external acoustic (incoherent) noise. PAS signals are proportional to the pump laser intensity and therefore PAS is most effective with high-power laser excitation. A sensitivity of 8 ppmv was demonstrated with only 2 mW of modulated diode laser power in the CH_4 overtone region [32, 33]. The implementation of DFB-QC laser excitation in the fundamental absorption region has the potential of considerably improved PAS detection sensitivity.

2.1. PHOTOACOUSTIC SPECTROSCOPIC TECHNIQUES

In 2001, D. Hofstetter et al. [34, 35] reported PAS measurements of ammonia, methanol and carbon dioxide using a pulsed DFB QC laser operated at 3–4% duty cycle with 25 ns long current pulses (2 mW average power) and Peltier cooling. Temperature tuning resulted in a wavelength range of 3 cm^{-1} with a linewidth of 0.2 cm^{-1}. This sensor used a 42 cm long PAS cell with a radial 16-microphone array for increased detection sensitivity. In addition the cell was placed between two concave reflectors resulting in 36 passes through the cell (with an effective pathlength of 15 m). The laser beam was chopped at a resonant cell frequency of 1.25 kHz, which resulted in a PAS signal enhancement by a Q factor of 70. Detection of ammonia concentrations at the 300 ppbv level with a SNR (Signal to noise ratio) of 3 was achieved at a pressure of 300 Torr.

Ammonia and water vapor photoacoustic spectra were obtained using a cw cryogenically cooled DFB QC laser with a 16 mW power output at 8.5 μm as reported in Ref. [36]. A PAS cell resonant at 1.66 kHz was used. Measured concentrations ranged from 2,200 ppmv to 100 ppbv. The microphone PAS signal was processed by a lock-in amplifier and normalized to the intensity measured by a HgCdTe detector. A detection limit of 100 ppbV ammonia ($\sim 10^{-5}$ noise-equivalent absorbance) at standard temperature and pressure was obtained for a 1 Hz bandwidth and a measurement interval of 10 min. Hence the sensitivity

obtained is comparable with that achieved by a direct absorption technique, but the required scan times are longer.

2.2. QUARTZ ENHANCED PHOTOACOUSTIC SPECTROSCOPIC TECHNIQUES

A recently introduced new approach to photoacoustic detection of trace gases utilizing a quartz tuning fork (QTF) as a sharply resonant acoustic transducer was first reported in 2002 [37, 38]. Advantages of a technique referred to quartz-enhanced photoacoustic spectroscopy (QEPAS) compared to conventional resonant photoacoustic spectroscopy include sensor immunity to environmental acoustic noise, a simple design of an absorption detection module, no requirement for a spectrally selective element, applicability over a wide range of pressures, including atmospheric pressure and the capability to analyze small gas samples, down to 1 mm^3 in volume. The measured normalized noise equivalent absorption coefficient for H_2O is $1.9 \times 10^{-9}\,cm^{-1}\,W/Hz^{-1/2}$ in the overtone region at $7306.75\,cm^{-1}$ which is the best detection sensitivity among the trace gas species tested to date using QEPAS and is indicative of fast vibrational – translational relaxation of initially excited states. An experimental study of the long-term stability of a QEPAS-based NH_3 sensor showed that the sensor exhibits very low drift, which allowed data averaging over >3 hours of continuous concentration measurements [38].

2.2.1. *Fundamentals of QEPAS*

QEPAS is an alternative approach to detecting a weak photoacoustic excitation. The basic idea of QEPAS is to invert the common PAS approach and accumulate the acoustic energy not in a gas-filled cell but in a sharply resonant acoustic transducer. Such an approach removes restrictions imposed on the gas cell by the acoustic resonance conditions. The transducer can be positioned in the acoustic near-field zone of the optical excitation beam, in which case the gas enclosure is optional and serves only to separate the gas sample from the environment and control its pressure.

Conventional microphones are not suitable for this task because they are designed for a flat frequency response. A natural candidate for such an application is crystal quartz, because it is a low-loss piezoelectric material. A variety of packaged quartz crystals for use in timing applications is commercially available. However, most of them resonate at megahertz frequencies and are therefore not appropriate to gas-phase PAS, because the energy transfer processes in gases occur on a longer time scale, and also because the PAS signal decreases at higher frequencies. Readily available low-frequency quartz elements are quartz tuning forks (QTF) intended for use in electronic clocks as frequency standards (Fig. 1). QTFs resonate at 32 768 (2^{15}) Hz in vacuum. Only the symmetric vibration of a QTF (i.e. the two tuning fork (TF) prongs bend in opposite directions) is

- Very small absorption detection module (ADM)
- Rugged transducer quartz monocrystal
- Ultrasmall sample volume – <1 mm^3
- Immune to environmental acoustic noise – acoustic quadrupole
- Sensitivity is limited by the fundamental thermal TF noise – k_BT energy in the TF symmetric mode, directly observed
- White noise spectrum – SNR scales as $\sqrt{t}$ up to t=3 hours

Figure 1. QEPAS based absorption detection module and merits of QEPAS based trace gas detection

piezoelectrically active. Hence the excitation beam should pass through the gap between the QTF prongs for efficient excitation of this vibration. Acoustically, a QTF is a quadrupole, which results in excellent environmental noise immunity. Sound waves from distant acoustic sources tend to move the QTF prongs in the same direction, thus resulting in no electrical response.

The QEPAS data acquisition system is similar to conventional PAS and was described in Ref. [38]. Most QEPAS studies reported to date have been performed using a wavelength modulation approach and $2f$ detection, which suppresses the background originating from spectrally nonselective absorbers (such as resonator walls, QTF electrodes, and the gas cell elements). The laser beam is focused between the prongs of the QTF and its wavelength is modulated at $f_m = f_0/2$ frequency, where f_0 is the QTF resonant frequency. A lock-in amplifier is used to demodulate the QTF response at f_0. Spectral data can be acquired if the laser wavelength is scanned. To increase the effective interaction length between the radiation-induced sound and the QTF, an acoustic gas-filled resonator can be added similarly to the traditional PAS approach.

Recently, Wojcik et al [39] demonstrated the performance of an infrared photoacoustic laser absorbance sensor for broadband gas-phase species with unresolved rotational spectral structure using an amplitude modulated (AM) quantum cascade (QC) laser and a QTF. A photoacoustic signal is generated by focusing 5.3 mW of a Fabry-Perot QC laser operating at 8.41 μm between the tines of a QTF. The sensitivity of this sensor was calibrated using the infrared absorber Freon-134a and performing simultaneous absorption measurements using a 31 cm absorption cell. The power and bandwidth normalized noise equivalent absorption sensitivity (NEAS) of this mid-infrared Freon 134a sensor was determined to be $2.0 \times 10^{-8}\ W \cdot cm^{-1}/\sqrt{Hz}$.

Analogous to conventional PAS, the QEPAS response, S to optical absorption is described by Equation (1),

$$S = k\frac{\alpha l C P Q}{f V} \tag{1}$$

where α is the absorption coefficient per unit concentration of the target trace gas species, C is the concentration of the target species, P is the applied optical power, f is the QEPAS sound frequency, V is the resonator volume and k is a constant describing other system parameters. The Q is a quality factor of the QTF and typically ranges from 10^4 to 10^5, depending on the carrier gas and the gas pressure. The minimum optical absorption coefficient detectable with a PAS based sensor is determined by the condition $S = N$, where N is the noise level (which is assumed to be independent of the optical excitation).

2.2.2. *Quartz tuning fork: resonant properties and noise*

QTFs can be designed to resonate at any frequency in the 10–150 kHz range and beyond, but we assume that a QTF with $f_0 = 32\,768$ Hz is used in QEPAS based sensors because of its commercial availability and low cost. Mechanical and electrical properties of QTFs were extensively studied in relation to their application in ultrahigh resolution scanning microscopy as reported in Ref [40–43].

The mechanical and electrical properties of the QTF are coupled via the piezoelectric effect. The QTF parameters as a mechanical oscillator correspond to equivalent electrical parameters of a series RLC circuit: mass (m) to inductance (L), rigidity (k) to inverse capacity ($1/C$) and damping β to resistance R. The resonant frequency f_0 and Q-factor of the QTF are related to R, L, and C as follows:

$$f_0 = \frac{1}{2\pi}\sqrt{\frac{k}{m}} = \frac{1}{2\pi}\sqrt{\frac{1}{LC}} \tag{2}$$

$$Q = \frac{1}{R}\sqrt{\frac{L}{C}} \tag{3}$$

A mechanical deformation of the QTF prongs induces electrical charges on its electrodes. A practical way to acquire the QTF electrical response is to utilize a trans-impedance amplifier. A gain resistor $R_g = 10\,\mathrm{M}\Omega$ is used in our design. In Ref [38] it was shown that the QEPAS noise measured at the amplifier output at the resonant frequency f_0, is equal to the theoretical thermal noise of the equivalent resistor R:

$$\frac{\sqrt{\langle V_N^2\rangle}}{\sqrt{\Delta f}} = R_g\sqrt{\frac{4k_B T}{R}} \tag{4}$$

where $\sqrt{\langle V_N^2 \rangle}$ is the RMS voltage noise at the trans-impedance amplifier output, Δf is the detection bandwidth, and T is the QTF temperature. The gain resistor R_g also introduces noise with a spectral density $\sqrt{4k_B T R_g}$, but it is $\sqrt{\frac{R_g}{R}}$ times lower than the QTF noise and can be usually neglected for typical values of $R \sim 10$–$100\,\mathrm{k}\Omega$.

2.2.3. *QEPAS implementation and observations*

A half-wave acoustic resonator can be added to increase the effective interaction length between the radiation-generated sound and the TF. It consists of two rigid tubes, each 2.45 mm long with a 0.32 mm inner diameter, aligned perpendicular to the TF plane. The distance between the free ends of the tubes was equal to half wavelength of sound in air at 32.75 kHz, thus satisfying the resonant condition [43]. Such a micro-resonator was found to enhance the QEPAS sensitivity ~8 to 10 times regardless of a ~0.4 mm wide gap between the tubes where the QTF was located. The presence of the resonator did not noticeably change the measured Q-factor of the QTF. All the measurements described below were performed using an ADM consisting of the QTF and such an acoustic micro-resonator.

The QEPAS sensitivity to the concentration of the trace component in a specific gas sample is a function of the sample pressure. This dependence is determined by the following characteristic trends:

1) TF Q-factor decreases at higher pressures. The SNR is proportional to $\sqrt{Q}$ for a fixed f_0 and applied mechanical force.
2) Peak optical absorption varies with pressure, especially at low (<30 Torr) pressures when collisional line broadening is less than Doppler broadening. On the other hand, merging of closely spaced absorption lines should be taken into account at higher pressures [45]
3) Energy transfer from vibrationally excited molecules to translational degrees of freedom (V-T relaxation) is faster at higher pressures, resulting in more efficient sound excitation. The effect of the V-T relaxation rate on the QEPAS signal is discussed in detail in [46]
4) Acoustic resonator enhancement factor changes with pressure.

The laser wavelength modulation amplitude $\Delta\lambda$ must be optimized at each pressure for the highest $2f$ signal. The two parameter optimization (pressure and $\Delta\lambda$) was reported for different gases in 45–48. It was experimentally found that the optimum $\Delta\lambda \approx 2 \times$ FWHM of the target absorption line.

The optical configuration of the QEPAS sensor should be designed so as to avoid laser illumination of the QTF and in particular on the inner surface of the acoustic micro-resonator, including any scattered light and incidental reflections from the optical elements. The $2f$ operation mode greatly reduces direct photothermal excitation of the QTF. In the practical implementation of the QEPAS

ADM the acoustic resonator mount serves as an efficient shield protecting the QTF from the scattered radiation. Tilting of the cell windows and proper laser beam shaping results in background-free trace gas detection.

2.2.4. *Review of QEPAS-based trace gas sensors*

The results reported so far in published QEPAS studies [45–49] are summarized in Table 2. The first six lines represent optical excitation in the overtone region, the seventh line is a CO_2 combination band transition and the other six lines refer to mid-infrared excitation of fundamental molecular vibrations.

NH_3 (Ref. [45]): The NNEA measured for this molecule in the overtone region is one of the best among the tested trace gas species to date, indicative of fast vibrational-translational (V-T) relaxation of initially excited states. Signal dependence on the gas pressure follows the product of the peak absorption, TF Q factor, and acoustic resonator enhancement factor, which confirms that the $2\pi f_0 \tau_{\text{V-T}} \ll 1$ condition ($\tau_{\text{V-T}}$ is the V-T energy transfer time constant) is satisfied at gas pressures >30 Torr. The highest detection sensitivity is achieved at a gas sample pressure of 60 Torr. The demonstrated QEPAS NNEA and NEC values

TABLE 2. QEPAS performance for 11 trace gas species.

Molecule (Host)	**Frequency, cm^{-1}**	**Pressure, Torr**	**NNEA, $cm^{-1}W/Hz^{1/2}$**	**Power, mW**	**NEC (τ=1 s), ppmv**
H_2O (N_2)**	7306.75	60	1.9×10^{-9}	9.5	0.09
HCN (air: 50% RH)*	6539.11	60	$<4.3 \times 10^{-9}$	50	0.16
C_2H_2 (N_2)**	6529.17	75	$\sim 2.5 \times 10^{-9}$	$\sim$40	0.06
NH_3 (N_2)*	6528.76	60	5.4×10^{-9}	38	0.50
CH_4 (N_2)*	6057.09	950	2.9×10^{-8}	13.7	2.1
CO_2	6361.25	90	1.6×10^{-8}	26	410
CO_2 ($N_2 + 1.5\%H2O$)*	4991.26	50	1.4×10^{-8}	4.4	18
CH_2O (N_2: 75%RH)*	2804.90	75	8.7×10^{-9}	7.2	0.12
CO (N_2)	2196.66	50	5.3×10^{-7}	13	0.5
CO (propylene)	2196.66	50	7.4×10^{-8}	6.5	0.14
N_2O(air + 5%SF_6)	2195.63	50	1.5×10^{-8}	19	0.007
C_2H_5OH**	1934.2	770	2.2×10^{-7}	10	90
C_2HF_5 (Freon125)***	1208.62	770	7.9×10^{-9}	6.6	0.009

* – Improved microresonator

** – Improved microresonator and double optical pass through ADM

*** – With amplitude modulation and metal microresonator

NNEA – normalized noise equivalent absorption coefficient.

NEC – noise equivalent concentration for available laser power and $\tau = 1$ s time constant.

for NH_3 compare very favorable with those reported for traditional PAS that use either a line-tunable CO_2 laser [50] or near-infrared diode laser fiber-amplifier source [51].
H_2O: The NNEA for this molecules is close to the NNEA measured for NH_3, also indicating a fast V-T relaxation of the excited states.
N_2O (Ref. [46]): The addition of SF_6 to the sampled air promotes the V-T relaxation and resulted in a 4 ppb NEC for $\tau = 3$ s time constant.
CO in N_2 (Ref. [46]): the V-T relaxation of the fundamental vibration of this molecule is too slow for efficient acoustic generation at 32.7 kHz. The observed QEPAS response is associated with fast rotational-translational relaxation of the rotational excitation accompanying absorption of the vibrational quantum.
CO in propylene, C_3H_6 (Ref. [49]): A propylene host was found to promote V-T relaxation of CO. However, the speed of sound in propylene is different from air (or N_2). Hence the acoustic resonator tube length no longer satisfies the resonant condition. Furthermore, the lock-in amplifier phase was set to suppress the background propylene signal and therefore the phase no longer coincides with the CO-originating photoacoustic signal.
CH_2O (Ref. [48]): The SNR was found to increase slowly for pressures >200 Torr.

We conclude from the above observations that the optimum pressure to detect molecules with isolated fast-relaxing optical transitions is ~50–90 Torr for the present ADM design. For slower relaxing species photoacoustic phase shift can enhance the chemical selectivity. This observation is not unique to QEPAS but is relevant to PAS in general. However, QEPAS operation at a high acoustic frequency, such as 32.7 kHz makes relaxation-related PAS phase shifts more pronounced. Observation of PAS phase shifts by means of a QTF can be an effective tool to study V-T relaxation processes in gases.

2.2.5. *Long term stability of QEPAS based trace gas sensors*

While the NNEA describes the sensor performance on a short time scale, other measurements are required to characterize long-term drifts and establish the signal averaging limits. We adopted an approach described in Ref. [52], which introduced the Allan variance of time sequences of measurements to quantify the long-term stability of optical trace gas sensors. A flow of nitrogen with 6 ppmv (parts per million by volume) NH_3 from a trace gas standard generator was passed through the QTF cell at a rate of 42 sccm. The gas pressure in the QTF cell was maintained at 60 Torr by means of a pressure controller. The laser radiation was alternatively locked to the NH_3 absorption line at 6528.76 cm^{-1} (ON mode) or detuned to an absorption-free region at ~6528.4 cm^{-1} (OFF mode).

ON and OFF modes were switched every 1200 s. As in Ref. [38], the laser power in the TF cell was 38 mW. The lock-in amplifier time constant was τ=1 s, and third order low-pass filter settings (18 dB/oct) were used. With these settings of the lock-in amplifier the directly measured equivalent noise bandwidth ENBW=0.19 Hz. The lock-in amplifier readings were recorded every 3 s, and the measurements performed continuously for ~16 hours. To perform an Allan variance analysis, all the data subsets with the laser on the absorption line were stacked together and treated as a single uninterrupted time sequence. A similar procedure was performed with the data subsets corresponding to the OFF mode. Then the laser beam was blocked, the lock-in amplifier time constant changed to τ=0.3 s (ENBW=0.63 Hz), and the lock-in amplifier readings were recorded every 1 s. The total duration of this experiment was ~15 h. The results of the Allan variance analysis are presented in Fig. 2. For clarity, the Allan deviation ($\sqrt{\langle\sigma_A^2\rangle}$) is shown instead of the variance, and expressed in terms of absorption coefficient or ammonia concentration for this particular sensor. ON and OFF mode data resulted in practically coincident plots, therefore only the ON mode data are shown. The initial deviation of the curves from the $1/\sqrt{t}$ dependence is caused by the correlation of the lock-in amplifier readings for ~8τ. The Allan deviation for all time sequences closely follows a $1/\sqrt{t}$ dependence over the entire duration of the measurements series. This observation verifies that white Johnson noise of the TF remains the dominant source of noise even on a multi-hour time scale, and the QEPAS based sensor allows practically unlimited data averaging without base line or sensitivity drift. For comparison, trace gas sensors based on direct optical

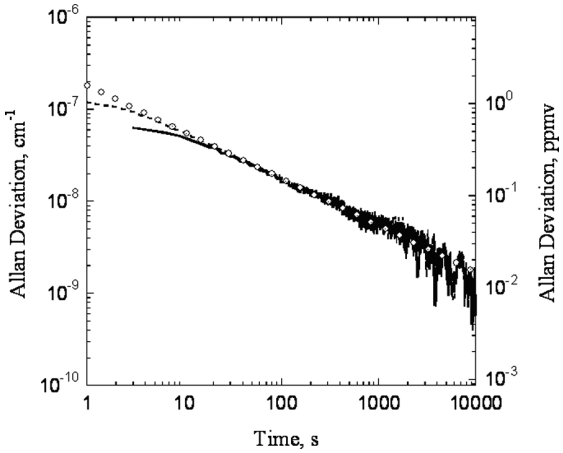

Figure 2. Allan deviation as a function of the data averaging period. Solid line: laser is locked to the NH_3 absorption line at 6528.4 cm^{-1}, lock-in amplifier time constant 1 s. Dotted line: laser beam is blocked, lock-in amplifier time constant 0.3 s. Open circles trace: $1/\sqrt{t}$ slope.

absorption detection usually exhibit drifts that do not allow useful data averaging for time periods longer than 100–200 s (see, for example, Ref. [53]).

2.3. QEPAS BASED CHEMICAL SENSOR ARCHITECTURE

The functional diagram of a recent configuration of a QEPAS based chemical gas sensor is shown in Fig. 3. The sensor utilizes a $2f$ wavelength-modulation spectroscopy approach, where $2f = f_0$ in the case of QEPAS. The sensor consists of several subsystems: the ADM with a trans-impedance amplifier (which has to be positioned close to the TF), a control and data processing electronics unit (CEU) schematically shown as a shaded box in Fig. 3, and a set of optical components including the excitation laser and reference cell with a photodetector. The optical components can vary depending on the spectral range, target molecule and the excitation laser. The laser wavelength is determined by the voltage applied to the laser driver input. For example, the wavelength of a distributed feedback semiconductor laser changes with current. The dc component of the laser current determines its central wavelength, whereas the sinusoidal ac component produces the wavelength modulation.

To make the CEU an integral part of the QEPAS gas sensor, the initial parameters must be set. This can be performed either from the front-panel keypad or via a RS232 serial interface. Parameters are stored in the CEU memory. A *LabView* driver was created for convenient initial setup and laboratory tests. The CEU was tested for C_2H_2 detection with 32.76 kHz and 20.0 kHz TFs (without acoustic resonator). The CEU performance was found to equal the performance of the laboratory setup which incorporated two commercial lock-in amplifiers (SR 830 DSP, Stanford Research Systems) and a computer-controlled function generator

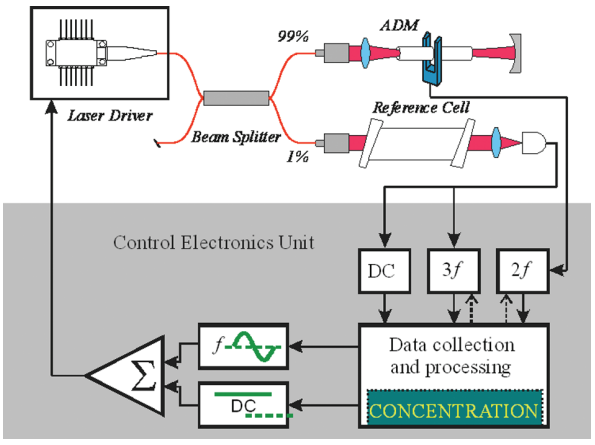

Figure 3. QEPAS fiber based gas sensor architecture.

(DS 345, Stanford Research Systems). The measured noise level matched the theoretically calculated TF noise within a 10% accuracy.

2.3.1. *QEPAS based ammonia detection with a near-infrared diode laser*

Trace ammonia quantification in the gas phase at different concentration levels is required in diverse areas of applications such as industrial process control, automotive exhaust analysis, medical diagnostics (kidney and liver dysfunctions), and environmental monitoring. One specific application that requires ammonia detection at ppm levels is the identification of leaks in industrial refrigeration systems.

The QEPAS sensor configuration is similar to that reported in earlier publications [37, 47] and is shown in Fig. 3. A 1.53 μm fiber-coupled DFB telecommunication diode laser serves as an excitation source for generating the QEPAS signal. A notebook computer with a data acquisition card and LABVIEW based software is used to collect data and control the dc voltage applied to the laser driver, as well as the ac component produced by a function generator. Fig 4 depicts the simulated NH_3 absorption spectrum in the near and mid-infrared spectral regions based on the Pacific Northwest National Laboratory spectroscopic data base. Clearly the best sensitivity can be obtained with absorption lines of the NH_3 fundamental ν_2 band at 10 μm.

For the actual ammonia detection, the laser modulation frequency f was set to half of the resonant frequency of the QTF, and the TF generated signal was rectified at $2f$ frequency by means of a lock-in amplifier. The laser wavelength can be either scanned to acquire $2f$ spectra, or locked to a selected absorption line for continuous concentration monitoring. Wavelength locking is performed with a

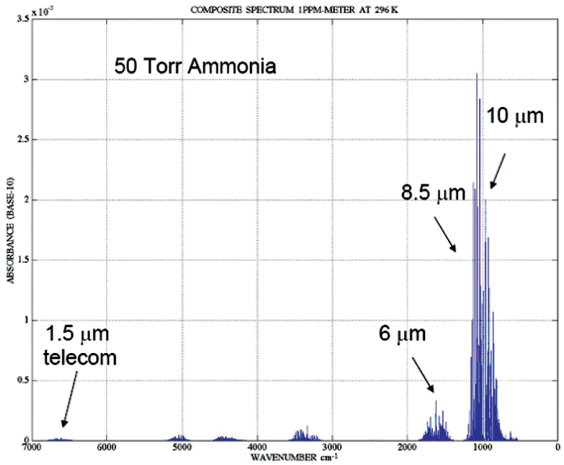

Figure 4. Simulated infrared NH_3 absorption spectrum.

common $3f$ approach. Namely, a small fraction of the laser radiation is directed through the reference gas cell containing NH_3 in nitrogen at a concentration ensuring 5% to 20% peak absorption at the target wavelength. The total pressure in the reference cell is ~2 times higher than the pressure in the TF gas cell. The signal from a photodiode PD (Fig. 3) was demodulated at a $3f$ frequency. The $3f$ component crossed zero at the line center, which allows the use of this signal as feedback in the wavelength stabilization loop. A permeation-tube based gas-standards generator was used to generate calibrated trace concentrations of NH_3 in pure N_2. All of the measurements were performed in gas flow to reduce adsorption–desorption effects, typically 50 sccm (cubic centimeters per minute at STP) N_2 mass-flow.

The ammonia concentration resulting in a noise-equivalent signal was found to be 0.5 ppm with 38-mW optical excitation power at 6528.76 cm^{-1} and a lock-in amplifier time constant of 1 s. This as mentioned above corresponds to a normalized absorption sensitivity of $5.4 \times 10^{-9}\,cm^{-1}\,W/Hz^{1/2}$, comparable with detection sensitivity achieved in conventional photoacoustic spectroscopy. [50, 51]

2.3.2. *Formaldehyde detection using an interband cascade laser at* 3.53 μm

Formaldehyde, which is an ubiquitous component of the lower atmosphere, is formed by the oxidation of most anthropogenic and biogenic hydrocarbons. H_2CO detection is of particular interest as a potential carcinogenic substance that is released from chemical binders present in numerous manufactured items and hence its presence in the environment cannot be avoided, particularly in poorly ventilated structures. NASA has established a spacecraft maximum allowable concentration level of <100 ppbv for crew exposures to H_2CO for extended periods of time. The Occupational Safety and Health Administration (OSHA) has issued general industrial safety standards with an upper limit of 750 ppb for long term exposure (8 hours) and 2 ppmv for short term exposures (15 minutes).

A novel continuous-wave, mid-infrared distributed feedback interband cascade laser was utilized to detect and quantify formaldehyde (H_2CO) using quartz enhanced photoacoustic spectroscopy [48]. The sensor architecture is depicted in Fig 5. The laser was operated at liquid-nitrogen temperatures and provides a single-mode output power of up to 12 mW at 3.53 μm (2832.5 cm^{-1}). The noise equivalent (1σ) detection sensitivity of the sensor was measured to be $1.1 \times 10^{-8}\,cm^{-1}W/Hz^{-1/2}$ for H_2CO in ambient air with 75% relative humidity, which corresponds to a detection limit of 0.20 ppmv for a 1 s sensor time constant and 4.6 mW laser power delivered to the QEPAS absorption detection module.

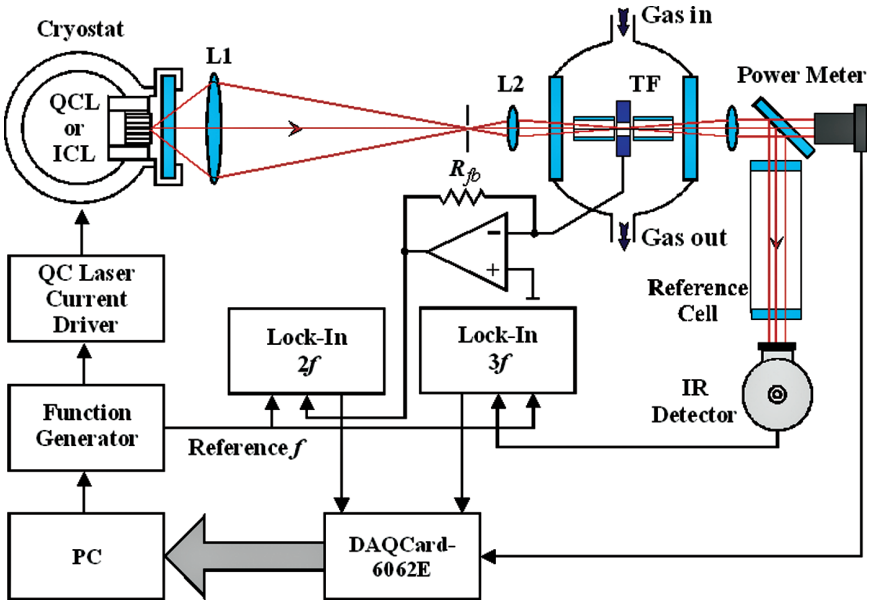

Figure 5. QCL or ICL based QEPAS trace gas sensor

3. Chemical sensing based on tunable thermoelectrically cooled CW quantum cascade lasers. Gas sensing with a cw DFB QC laser was first reported in Ref. [54].

3.1. DETECTION OF TRACE GASES WITH WIDELY TUNABLE QC LASERS

3.1.1. *NO detection using widely tunable external cavity QC laser at* $\sim$5.2 μm

The development of laser spectroscopic techniques strongly relies on increasing the availability of new tunable laser sources. For applications in the mid-infrared (mid-IR) molecular fingerprint region, quantum cascade lasers (QCLs) have proved to be convenient and reliable light sources for the spectroscopic detection of trace gases [55]. Spectroscopic applications usually require single frequency operation. This is achieved by introducing a distributed feedback (DFB) structure into the QCL active region. Although DFB QCLs show high performance and reliability, the range of wavelength tuning of the emitted laser radiation is limited by the limited tuning range of the DFB structures. Typically the maximum thermal tuning range of DFB-QCLs is $\sim$2 cm^{-1} achieved by laser current injection control or $\sim$10 cm^{-1} by varying the temperature of the QCL chip. One of the disadvantages of such a thermal tuning is that it affects the effective gain of the QCL, which consequently causes a decrease of the output laser power with increasing temperature of the QCL chip. Recently several groups have reported progress in the

development of continuous wave (cw) QCLs operating at temperatures accessible with thermoelectric cooling. In particular the development of bound-to-continuum QC lasers [56] has greatly alleviated both of these impediments to wide frequency tuning. Bound-to-continuum QC lasers have an intrinsically broader gain profile because the lower state of the laser transition is a relatively broad continuum. A luminescence spectrum of 297 cm^{-1} FWHM (full width at half maximum) at room temperature was observed for $\lambda = 10\mu m$ QCL devices employing bound-to-continuum transitions. Recently even broader gain profiles with a FWHM of $\sim$350 cm^{-1} were achieved appling heterogonous quantum-cascade structure based on two bound-to-continuum designs emitting at 8.4 μm and 9.6 μm [57]. To take advantage of the broadband gain of such QCLs, an external cavity (EC) configuration can be used for wavelength selection [58]. This work reports on the development of a QC laser spectrometer for high resolution spectroscopic applications and multi species trace-gas detection in the mid-infrared through the design and implementation of a novel EC-QCL architecture. The instrument employs a piezo-activated cavity mode tracking system for modehop free operation. The mode-tracking system provides independent control of the EC length diffraction grating angle and QC laser current. The flexibility of this arrangement allows the instrument to be used with other QC lasers at other wavelengths without changing the EC configuration. The system performance and spectroscopic application capability is demonstrated with a gain medium fabricated using a bound-to-continuum design and operating at $\sim$5.2 μm.

3.2. EC-QCL SYSTEM CONFIGURATION

Detection of nitric oxide (NO) is important in many applications that include industrial emission and process monitoring [59], atmospheric research [60], and medical diagnostics [61–64]. These applications benefit from the availability of an external cavity (EC) quantum cascade laser configuration with a thermoelectrically cooled gain medium fabricated using a bound-to-continuum design and operating in continuous wave at $\sim$5.2 μm which was realized in 2005 [30]. The EC-QCL architecture as depicted in Fig. 6 employs a piezo-activated cavity mode tracking system for mode-hop free operation. The system provides independent wavelength tracking by all three wavelength-selective elements of the EC-QCL architecture: QCL cavity, EC and diffraction grating. The performance of the EC-QCL exhibits coarse single mode tuning over 35 cm^{-1} and a continuous mode-hop free fine tuning range of $\sim$1.2 cm^{-1} is shown in Fig. 7. Wide tunability and a narrow laser linewidth of $<$30 MHz, which allowed resolving spectral features separated by less than 0.006 cm^{-1} (see inset of Fig. 7) makes the EC-QCL an excellent light source suitable for high resolution spectroscopic applications and multiple species trace-gas detection.

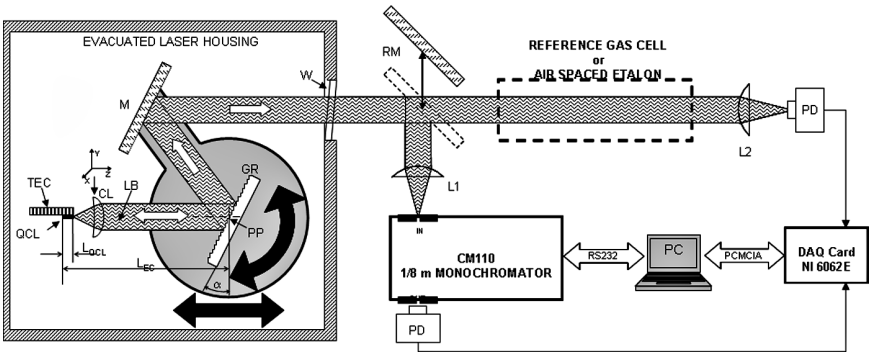

Figure 6. Schematic diagram of the EC QCL laser and the associated measurement system. QCL – quantum cascade laser, TEC – thermoelectric cooler, CL – collimating lens (1″ diameter, f/0.6, Ge AR-coated 3–12 μm) mounted on a motorized 3D translation stage, LB –laser beam, GR – diffraction grating (150 gr/mm blazed for 5.4 μm), PP – pivot point of the rotational movement, M – mirror (mounted on the same platform with GR), W – CaF_2 window (thickness 4mm, tilted ∼5°), RM – removable mirror, PD –photodetector (Hg-Cd-Zn-Te, TE-cooled, Vigo Systems, PDI-2TE-6), L1, L2 – ZnSe lenses.

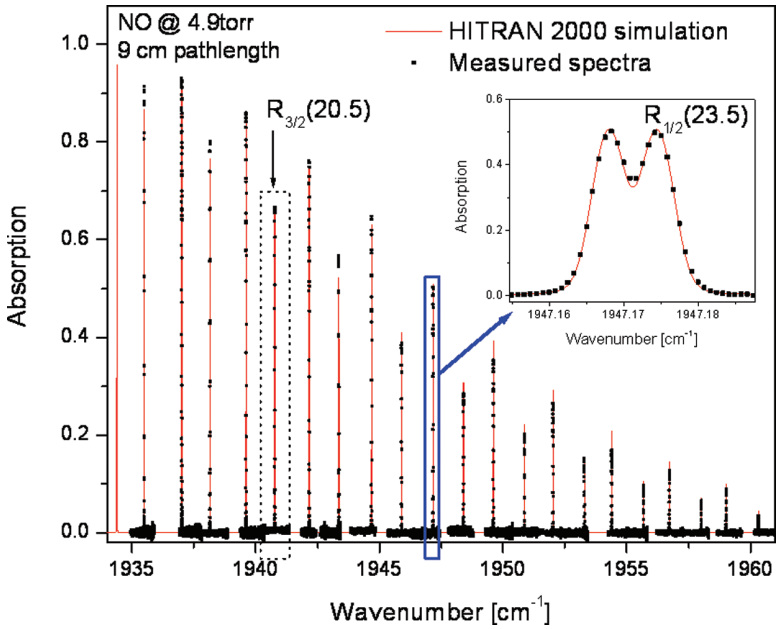

Figure 7. Nitric oxide absorption spectra measured at different diffraction grating angles of the external cavity quantum cascade laser. The narrow laser linewidth allows resolving two spectral peaks separated by $\sim 0.006\,\mathrm{cm}^{-1}$ (see inset).

The complete laser cavity can be analyzed as a system of two coupled cavities: the QCL chip cavity between back and front facet of the QCL and the external cavity which consist of the HR coated back facet and the diffraction grating. The optical length of the QCL cavity is $L_{\mathrm{QCL}} = n_{\mathrm{CQL}} \times l = \sim 1$ cm where n_{QCL} is the refractive index of the chip material and l is its length. The average optical length of the external cavity is ~9.3 cm. This results in a free spectral range (FSR) of 0.5 cm^{-1} (15 GHz) for the QCL. The EC Fabry–Perot (FP) resonator has an FSR of 0.053 cm^{-1} (1.6 GHz). The diffraction grating acts as a band pass filter, for which the bandwidth can be estimated by calculating its resolving power

$$\Delta\lambda = \frac{\lambda}{|m|\,N} = \frac{\lambda d \cos\alpha}{a} \tag{5}$$

where λ represents the wavelength, $m = 1$ is a diffraction order, N is the number of grating lines illuminated, a is a diameter of the collimated laser beam and ψ is the incident angle of the beam measured between the grating normal and the optical axis of the beam. For our system, where $\lambda = 5.2\,\mu$m, $d = 6.67\,\mu$m, $a = \sim 20$ mm and $a = 22.95$ the approximation yields $\Delta\lambda = \sim 1.6$ nm (~0.6 cm^{-1}, ~17.7 GHz).

To demonstrate the capability of multi species concentration measurements within a single scan, a reference cell, which contained some residual H_2O, was evacuated for a short period of time and subsequently filled with pure NO (with a partial pressure of 5 Torr). The H_2O absorption lines at 1942.52 cm^{-1} and 1942.76 cm^{-1} were measured along with the NO–$R_{3/2}$ (21.5) line at 1943.36 cm^{-1}. The measured data together with a simulated spectrum is plotted in Fig. 8. The simulation gives a partial pressure of H_2O of ~7 Torr. The background spectrum was measured with the reference cell removed from the optical path. This causes the effective path length in the atmosphere to increase by the reference cell length. The negative envelope around the water lines corresponds to an absorption spectrum of atmospheric H_2O within this additional pathlength. In the composite plot, the effects of pressure broadening and frequency shift are also observable.

4. Trace gas sensors using a high-finesse optical cavity

Sensitive laser absorption spectroscopy often requires a long effective pathlength of the probing laser beam in media being analyzed. Traditionally, this requirement is satisfied using an optical multipass cell. Such an approach has a number of shortcomings, especially for compact gas sensor configurations. Multipass cells tend to be bulky requiring a large footprint. For example, a typical commercial 100 m pathlength multipass cell has a volume of 3.5 liters. Such gas absorption cells also require costly large-aperture mirrors sometimes with aspheric surfaces.

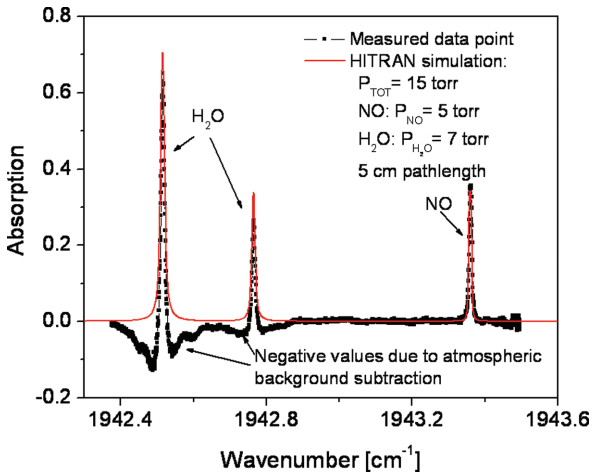

Figure 8. Single spectral scan of NO and strong neighboring H_2O lines. Background measurement was performed with the reference gas cell removed from the beam path. Therefore negative values of the calculated absorption spectrum are visible, which corresponds to reduced atmospheric water absorption (the negative part is related to a pressure broadened H_2O spectrum at atmospheric pressure).

An alternative way to obtain a long optical path is to make the light bounce along the same path between two parallel ultralow-loss dielectric mirrors. An effective optical pathlength of several kilometers can be obtained in a very small volume. The light leaking out of such an optical cavity can be used to characterize the absorption of the intracavity medium. Presently a variety of techniques exists to perform high-sensitivity absorption spectroscopy in a high finesse optical cavity (for example, see Ref. [20]). One of the most advanced method is the so-called "Noise-Immune Cavity-Enhanced Optical Heterodyne Molecular Spectroscopy" (NICE-OHMS) technique [65]. It has the potential to provide shot-noise limited sensitivity with an effective pathlength determined by the cavity ringdown time. The first implementation of this technique in combination with a DFB-QC laser is reported in Ref. [66]. However, this approach is technically sophisticated and therefore not suitable for most practical chemical-sensing applications. Two simpler methods are cavity ringdown spectroscopy (CRDS) described in Part IV-4 and integrated cavity output spectroscopy (ICOS).

4.1. CAVITY RINGDOWN SPECTROSCOPY

The first CRDS measurements with a QC-DFB laser were reported in 2000 [67]. The authors used a cw laser generating 16 mW at $\lambda = 8.5\,\mu$m. The measured ringdown time of the empty three-mirror cavity was 0.93 μs. An acousto-optic modulator was used to interrupt the cavity injection for ringdown time measurements. The system was tested on diluted NH_3 mixtures. A noise-equivalent

sensitivity of 0.25 ppbv and an estimated $1.0 \times 10^{-9}\,\mathrm{cm}^{-1}$ detectable limit of the absorption coefficient were reported. Spectroscopic detection of ethane in the 3 μm wavelength region was achieved using a cw optical parametric oscillator and CRDS [68].

NO detection using CRDS at 5.2 μ*m*

NO is the major oxide of nitrogen formed during high-temperature combustion as well as an important nitrogen-containing species in the atmosphere (NO is a precursor of smog and acid rain). NO is also involved in a number of vital physiological processes, and its detection in exhaled breath has potential applications (e.g. as a biomarker for a number of lung diseases like lower-airway inflammation or asthma) in noninvasive medical diagnostics (see also Part IV-4).

A spectroscopic gas sensor for nitric oxide detection based on a cavity ringdown technique was reported in Ref. [69]. A cw quantum-cascade distributed-feedback laser operating at 5.2 μm was used as a tunable single-frequency light source. Both laser-frequency tuning and abrupt interruptions of the laser radiation were performed by manipulation of the laser current. A single ringdown event sensitivity to absorption of $2.2 \times 10^{-8}\,\mathrm{cm}^{-1}$ was achieved. Concentration measurements of ppbv levels of NO in N_2 with a 0.7-ppb standard error for a data collection time of 8 s was achieved.

4.2. CAVITY ENHANCED ABSORPTION SPECTROSCOPY

A gas analyzer based on a continuous-wave mid-infrared quantum cascade laser operating at ∼5.2 μm and on off-axis integrated cavity output spectroscopy (OA-ICOS) has been developed to measure NO concentrations in human breath [21]. A compact sample cell, 5.3 cm in length and with a volume of (80 cm^3, which is suitable for on-line and off-line measurements during a single breath cycle, was designed and tested. A noise-equivalent (signal-to-noise ratio of 1) sensitivity of 10 ppbv of NO was achieved. The combination of ICOS with wavelength modulation resulted in a 2-ppbv noise-equivalent sensitivity. The total data acquisition and averaging time was 15 s in both cases. M.L Silva et al [70] demonstrated a pulsed, non-cryogenic cavity-enhanced spectrometer that also operates at 5.2 μm.

Subsequently, a nitric oxide sensor based on a thermoelectrically cooled, cw DFB QCL laser operating at 5.45 μm (1835 cm^{-1}) and off-axis ICOS combined with a wavelength-modulation technique was developed to determine NO concentrations at the sub-ppbv levels that are essential for a number of applications, such as medical diagnostics (specifically in detecting NO in exhaled human breath) and environmental monitoring. The sensor employs a 50-cm-long high-finesse optical cavity that provides an effective path length of 700 m. A noise equivalent minimum detection limit of 0.7 ppbv with a 1-s observation time was achieved [71,72]. More recently [73], a detection sensitivity of 0.03 ppbv was achieved with 30 s

averaging time with a path length of 210 m, corresponding to an absorbance path length product of $1.5 \times 10^{-10}\,\mathrm{cm}^{-1}$.

Detection of formaldehyde using off-axis ICOS with a 12 mW interband cascade laser (ICL) was recently demonstrated [74] A 3.53 μm continuous-wave, mid-infrared, distributed feedback ICL was used to quantify H_2CO in gas mixtures containing ≈1–25 ppmv of H_2CO. Analysis of the spectral measurements indicates that a H_2CO concentration of 150 ppbv would produce a spectrum with a signal to noise ratio of 3 for a data acquisition time of 3 s. This is a minimum detection sensitivity level for formaldehyde monitoring of indoor air, industrial occupational settings, and on board spacecraft in long duration missions in particular as the detection sensitivity improves with the square root of the data acquisition time.

5. Conclusions

Progress to-date in terms of performance optimization of various cw and pulsed single frequency QC and IC laser based trace gas sensors as well as cw DFB diode lasers that use different sensitivity enhancement schemes and achieve minimum detectable absorbances (10^{-4} to 10^{-6}) limited by laser, optical and detector noise sources have been described. Compact, sensitive, and selective gas sensors based on mid-infrared QCLs and ICLs have been demonstrated to be effective in numerous applications since 1998. These now include such diverse fields as environmental monitoring (e.g CO, CO_2, CH_4 and H_2CO are important C_y gases in global warming and ozone depletion studies), industrial emission measurements (e.g. fence line perimeter monitoring in the petrochemical industry, combustion sites, waste incinerators, down gas well monitoring, gas pipeline and compressor station safety), urban (e.g. automobile traffic, power generation) and rural emissions (e.g. horticultural greenhouses, fruit storage and rice agro-ecosystems), chemical analysis and control for manufacturing processes (e.g. semiconductor, pharmaceutical, food), detection of medically important molecules (e.g. NO, CO, CO_2, NH_3, C_2H_6 and CS_2), toxic gases, drugs, and explosives relevant to law enforcement and public safety, and spacecraft habitat air-quality and planetary atmospheric science (e.g. such planetary gases as H_2O, CH_4, CO, CO_2 and C_2H_2).

To date, QC laser-based chemical sensors primarily use InGaAs/InAlAs type-I QC-DFB devices. There are two limitations inherent to this kind of lasers for chemical sensing. First, they cannot access the spectral region of C-H, O-H and N-H stretch vibrations near $3000\,\mathrm{cm}^{-1}$. This shortcoming can be overcome by developing QC lasers based on alternative materials and structures. For example, the $3000\,\mathrm{cm}^{-1}$ region is accessible by IC lasers or integrated parametric frequency converted type I QCL structures. Another issue is the limited wavelength tunability of each QC-DFB laser, which restricts the feasibility of probing the entire

molecular absorption spectrum, especially of volatile organic compounds and hydrocarbons as well as multi-component chemical sensing. This requirement can now be addressed by separating the gain medium from the wavelength-selective element. In Ref. [30] a QC laser tunability of $\sim$35 cm^{-1} at a fixed temperature was demonstrated in an external cavity configuration with a diffraction grating. This is $\sim$ ten times wider range than typically achieved for DFB-QC lasers by means of current tuning. In 2002 an ultra-broadband laser medium based on a number of combined dissimilar intersubband optical transitions was reported [75]. This medium can provide optical gain from 5 to 8 μm wavelength, which corresponds to a potential QC gain bandwidth of $>$400 cm^{-1}. Recently we were able to increase the overall tuning range from 35 cm^{-1} to 155 cm^{-1} at 5.2 μm and at 8.4 μm we obtained tunability of 135 cm^{-1} with a maximum single frequency output of 50 mW [76] using a QCL gain chip grown by a low-pressure metal organic vapor-phase epitaxy process [Ref. [13]].

Acknowledgments

The authors thank Dr. Robert F. Curl for numerous useful discussions and support of this work. We are also grateful to Drs. C. Gmachl, F. Capasso, L. Diehl, M. Troccoli, J. Faist, R. Maulini and R. Yang for their invaluable scientific support. Financial support of the research performed by the Rice group was provided by the National Aeronautics and Space Administration via awards from the Jet Propulsion Laboratory Pasadena, CA and Johnson Space Center, Houston, TX, the Pacific Northwest National Laboratory, Richland, WA, the National Science Foundation (ERC-MIRTHE), the Robert Welch Foundation, the Texas Advanced Technology Program and the Office of Naval Research via a sub-award of Texas A&M University.

References

1. F. K. Tittel, D. Richter and A. Fried, Mid-Infrared Laser Applications in Spectroscopy", *Solid State Mid-Infrared Laser Sources*, I. T Sorokina and K. L. Vodopyanov (Eds), Springer Verlag, Topics Appl. Phys. 89, 445–510 (2003).
2. R. F. Curl and F. K. Tittel, "Tunable Infrared Laser spectroscopy" *Ann.Rep.Prog.Chem., Sect*. C 98, 219–272 (2002).
3. T. Yanagawa, H. Kanbara, O. Tadanaga, M. Asobe, H. Suzuki, and J. Yumoto Broadband difference frequency generation around phase-match singularity, *Appl. Phys. Lett*. 86, 161106 (2005).
4. D. Richter and P. Weibring, Ultra high precision mid-IR spectrometer: design and analysis of an optical fiber pumped difference frequency generation source, *Appl. Phys. B* 82, 479–486 (2006).
5. P. Weibring, D. Richter, A. Fried, J. G. Walega, and C. Dyroff, "Ultra-high-precision mid-IR spectrometer II: system description and spectroscopic performance", *Appl. Phys. B* 85, 207–218, (2006).

6. A. A. Kosterev and F. K. Tittel, Chemical Sensors Based on Quantum Cascade Lasers, *IEEE JQE Special Issue on QC Lasers* 38, 582–591 (2002).
7. F. Capasso, C. Gmachl, R. Paiella, A. Tredicucci, A. L. Hutchinson, D. L. Sivco, J. N. Baillargeon, and A. Y. Cho, New Frontiers in Quantum Cascade Lasers and Applications, *IEEE Selected Topics in Quantum Electronics* 6, 931–947 (2000) and references therein.
8. J. Faist, D. Hofstetter, M. Beck, T. Aellen, M. Rochat, and S. Blaser, Bound-to-continuum and two-phonon resonance quantum-cascade lasers for high duty cycle, high temperature operation, *IEEE Journal of Quantum Electronics* 38, 533–546 (2002).
9. M. Beck, D. Hofstetter, T. Aellen, J. Faist, U. Oesterle, M. Ilegems, E. Gini, and H. Melchior, "Continuous wave operation of a mid-infrared semiconductor laser at room temperature", *Science* 295, 301–305 (2002).
10. Ch. Mann, Q. K. Yang, F. Fuchs, W. Bronner, R. Kiefer, K. Koehler, H. Schneider, R. Kormann, H. Fischer, T. Gensty, and W. Elsaesser, Quantum cascade lasers for the mid-infrared spectral range: devices and applications, B. *Adv. in Solid State Phys.* Kramer (Ed.), Springer Verlag 43, 351–368 (2003).
11. A. Evans, J. S. Yu, S. Slivken, and M. Razeghi, Continuous-wave operation of $\lambda \sim 4.8\,\mu m$ quantum-cascade lasers at room temperature, *Appl. Phys. Lett.* 85, 2166–2168 (2004).
12. M. Troccoli, D. Bour, S. Corzine, G. Hofler, A. Tandon, D. Mars, D. J. Smith, L. Diehl, and F. Capasso, Low-threshold continuous-wave operation of quantum-cascade lasers grown by metalorganic vapor phase epitaxy, *Appl. Phys. Lett*. 85, 5842–5844, (2004).
13. L. Diehl, D. Bour, S. Corzine, J. Zhu, G. Hoefler, M. Loncar, M. Troccoli, and F. Capasso, High-power quantum cascade lasers grown by low-pressure metal organic vapor-phase epitaxy operating in continuous wave above 400 K, Appl. Phys Lett. 88, 201115 (2006).
14. R. Q. Yang, J. L. Bradshaw, J. D. Bruno, J. T. Pham, and D. E. Wortman, " Mid-infrared type II interband cascade lasers, *IEEE J. of Quant. Elect.* 38, 547–558 (2002).
15. R. Q. Yang , C. J. Hill, B. H. Yang, C. M. Wong, R. E. Muller, and P. M. Echternach, Continuous-wave operation of distributed feedback interband cascade lasers, *Appl. Phys. Lett.* 84, 3699–3701 (2004).
16. J. L. Bradshaw, N. P. Breznay, J. D. Bruno, J. M. Gomes, J. T. Pham, F. J. Towner, D. E. Wortman, R. L. Tober, C. J. Monroy, and K. A. Olver, *Physica E* 20, 479 (2004).
17. K. Mansour, Y. Qiu, C. J. Hill, A. Soibel, and R. Q. Yang, Mid-infrared interband cascade lasers at thermoelectric cooler temperatures, *Electr. Lett.*. 42, 1034–1036 (2006).
18. L. Hvozdara, S. Gianordoli, G. Strasser, W. Schrenk, K. Unterrainer, E. Gornik, C. S. S. S. Murthy, M. Kraft, V. Pustogow, B. Mizaikoff, A. Inberg, and N. Croitoru, Spectroscopy in the gas phase with GaAs/AlGaAs quantum-cascade lasers, *Appl. Opt.* 39, 6926–6930 (2000).
19. C. Sirtori, H. Page, C. Becker, and V. Ortiz, GaAs-A1GaAs quantum cascade laser: physics, technology, and prospects, *IEEE Journal of Quantum Electronics* 38, 559–568 (2002).
20. G. Berden, R. Peeters, and G. Meijer, Cavity ring-down spectroscopy: Experimental schemes and applications, *Int. Reviews in Phys. Chemistry* 19, 565–607 (2000).
21. Y. A. Bakhirkin, A. A. Kosterev, C. Roller, R. F. Curl, and F. K. Tittel, Mid-Infrared Quantum Cascade Laser based Off-Axis Integrated Cavity Output Spectroscopy for Biogenic NO Detection. *Appl. Opt.* 43, 2257–2266 (2004).
22. C. R. Webster, G. J. Flesch, D. C. Scott, J. E. Swanson, R. D. May, W. S. Woodward, C. Gmachl, F. Capasso, D. L. Sivco, J. N. Baillargeon, A. L. Hutchinson, and A. Y. Cho, Quantum-cascade laser measurements of stratospheric methane and nitrous oxide, *Appl. Opt* 40, 321–326 (2001).

23. T. L. Myers, R. M. Williams, M. S. Taubman, F. Capasso, C. Gmachl, D. L. Sivco, J. N. Baillargeon, and A. Y Cho, Free-running frequency stability of mid-infrared quantum cascade lasers. *Optics Letters* 27, 170–172 (2002).

24. M. S. Taubmann, T. L. Myers, B. D. Cannon, R. M. Wiliams, F. Capasso, C. Gmachl, D. L. Sivco, and A. Y. Cho, Frequency stabilization of quantum cascade laser using optical cavities, *Opt. Lett*. 27, 2164–2166 (2002).

25. K. Namjou, S. Cai, E.A. Whittaker, J. Faist, C. Gmachl, F. Capasso, D. L. Sivco, and A. Y. Cho, Sensitive absorption spectroscopy with a room-temperature distributed-feedback quantum-cascade laser, *Opt. Lett*. 23, 219–221 (1998).

26. D. Hofstetter, M. Beck, T. Aellen, J. Faist, U. Oesterle, M. Ilegems, E. Gini, and H. Melchior, Continuous wave operation of a 9.3 μm quantum cascade laser on a Peltier coolant, *Appl. Phys. Lett,* 78, 1964–1966 (2001).

27. D. Weidmann, F. K. Tittel, T. Aellen, M. Beck, D. Hofstetter, J. Faist, and S. Blaser, Mid infrared trace gas sensing with a quasi-continuous wave Peltier-cooled distributive feedback quantum cascade laser, *App. Phys. B* 79, 907–913 (2004).

28. C. Peng, G. Luo, and H. Q. Le, Broadband, continuous, and fine-tune properties of external-cavity thermoelectric-stabilized mid-infrared quantum-cascade lasers, *Appl. Opt*. 42, 4877–4882 (2003).

29. R. Maulini, M. Beck, and J. Faist, Broadband tuning of external cavity bound-to-contimuum quantum-cascade lasers, *Appl. Phys. Lett*. 84, 1659–1661 (2004).

30. G. Wysocki, R. F. Curl, F. K. Tittel, R. Maulini, J. M. Bulliard, and J. Faist, Widely Tunable Mode-hop Free External Cavity Quantum Cascade Laser for High Resolution Spectroscopic Applications, *Appl. Phys. B* 81, 769–777 (2005).

31. M. Pushkarsky, A. Tsekoun, I. G. Dunayevskiy, R. Go, and C. K. N. Patel, Sub-parts-per-billion level detection of NO_2 using room-temperature quantum cascade lasers, *PNAS* 103, 10846–10849 (2006).

32. Geng-Chiau Liang, Hon-Huei Liu, A. H. Kung, A. Mohacsi, A. Miklos, and P. Hess, Photo-acoustic trace detection of methane using compact solid-state lasers, *J. Phys. Chem. A* 104, 10179–10183 (2000).

33. M. G.omes Da Silva, A. Miklos, A. Falkenroth, and P. Hess, Photoacoustic measurement of N_2O concentrations in ambient air with a pulsed optical parametric oscillator, *Appl. Phys. B* 82, 329–336 (2006).

34. D. Hofstetter, M. Beck, J. Faist, M. Naegele, and M. W. Sigrist, Photoacoustic spectroscopy with quantum cascade distributed-feedback lasers, *Opt. Lett.* 26, 887–889 (2001).

35. M. Nägele, D. Hofstetter, J. Faist, and M. W. Sigrist, Low power quantum-cascade laser photoacoustic spectrometer for trace-gas monitoring, *Analytical Sciences* 17 Special Issue, 497–499 (2001).

36. B. A. Paldus, T. G. Spence, R. N. Zare, J. Oomens, F. J. M. Harren, D. H. Parker, C. Gmachl, F. Capasso, D. L. Sivco, J. N. Baillargeon, A. L. Hutchinson, and A. Y. Cho, Photoacoustic spectroscopy using quantum-cascade lasers, *Opt. Lett.* 24, 178–180 (1999).

37. A. A. Kosterev, Y. A. Bakhirkin, R. F. Curl, and F. K. Tittel, Quartz-Enhanced Photoacoustic Spectroscopy, *Opt Lett.* 27, 1902–1904 (2002).

38. A. A. Kosterev, F. K. Tittel, D. Serebryakov, A. Malinovsky, and A. Morozov, Applications of Quartz Tuning Fork in Spectroscopic Gas Sensing, *Rev. of Sci. Instrum.* 76, 043105 (2005).

39. M. D. Wojcik, M. C. Phillips, B. D. Cannon, and M. S. Taubman, Gas Phase Photoacoustic Sensor at 8.41 μm Using Quartz Tuning Forks and Amplitude Modulated Quantum Cascade Lasers. *Appl. Phys. B.*. 85, 307–313. (2006).

40. K. Karrai and R. D. Grober, Piezoelectric tip-sample distance control for near field optical microscopes, *Appl. Phys. Lett*. 66, 1842–1844 (1995).

41. D. V. Serebryakov, A. P. Cherkun, B. A. Loginov, and V. S. Letokhov, Tuning-fork-based fast highly sensitive surface-contact sensor for atomic force microscopy/near-field scanning optical microscopy, *Rev. Sci. Instrum.* 73, 1795–1802 (2002).

42. T. Akiyama, U. Staufer, N. F. de Rooij, P. Frederix, and A. Engel, Symmetrically arranged quartz tuning fork with soft cantilever for intermittent contact mode atomic force microscopy, *Rev. Sci. Instrum*. 74, 112–117 (2003).

43. A. P. Cherkun, D. V. Serebryakov, S. K. Sekatskii, I. V. Morozov, and V.S. Letokhov, Double-resonance probe for near-field scanning optical microscopy, *Rev. Sci. Instrum* 77, 033703 (2006).

44. A. Miklos, P. Hess, and Z. Bozoki, Application of acoustic resonators in photoacoustic trace gas analysis and metrology, *Rev. Sci. Instrum*. 72, 1937 (2001).

45. A. A. Kosterev and F. K. Tittel, Ammonia detection by use of quartz-enhanced photoacoustic spectroscopy with a near-IR telecommunication diode laser, *Appl. Opt*. 43, 6213–6217 (2004).

46. A. A. Kosterev, Y. A. Bakhirkin, and F. K. Tittel, Ultra sensitive gas detection by quartz-enhanced photoacoustic spectroscopy in the fundamental molecular absorption bands region, *Appl. Phys.* B 80, 133–138 (2005).

47. D. Weidmann, A.A. Kosterev, F.K. Tittel, N. Ryan, and D. McDonald, Application of widely electrically tunable diode laser to chemical gas sensing with quartz-enhanced photoacoustic spectroscopy, *Optics Letters* 29, 1837–1839 (2004).

48. M. Horstjann, Y. A. Bakhirkin, A. A. Kosterev, R. F. Curl, and F. K. Tittel, Formaldehyde sensor using interband cascade laser based quartz-enhanced photoacoustic spectroscopy, *Appl. Phys. B,* 79, 799–803 (2004).

49. A. A. Kosterev, Y. A. Bakhirkin, F. K. Tittel, S. Blaser, Y. Bonetti, and L. Hvozdara, Photoacoustic phase shift as a chemically selective spectroscopic parameter, *Applied Physics B, (Rapid Communications)*, 78, 673–676 (2004).

50. M. E. Webber, M. Pusharsky, and C. K. N. Patel, Ultra-sensitive ambient ammonia detection using CO2-laser-based photoacoustic spectroscopy, *Applied Physics B* 77, 381–385 (2003).

51. M. E. Webber, T. MacDonald, M. B. Pushkarsky, and C. K. N. Patel, Agricultural ammonia sensor using diode lasers and photoacoustic spectroscopy, *Meas. Sci. Technol.* 16, 1547–1553 (2005).

52. P. Werle, R. Mücke, and F. Slemr, The Limits of Signal Averaging in Atmospheric Trace Gas Monitoring by Tunable Diode-Laser Absorption Spectroscopy, *Appl. Phys. B 57*, 131–139 (1993).

53. B. P. Wert, A. Fried, S. Rauenbuehler, J. Walega, and B. Henry, Design and performance of a tunable diode laser absorption spectrometer for airborne formaldehyde measurements, *J. Geophys. Res. 108*, 4350 (2003).

54. S. W. Sharpe, J. F. Kelly, J. S. Hartman, C. Gmachl, F. Capasso, D. L. Sivco, J. N. Baillargeon, and A. Y. Cho, High-resolution (Doppler-limited) spectroscopy using quantum-cascade distributed-feedback lasers, *Opt. Lett*. 23, 1396–1398 (1998).

55. G. Wysocki, A. A. Kosterev, and F. K. Tittel, Spectroscopic Trace-gas Sensor with Rapidly Scanned Wavelengths of a Pulsed Quantum Cascade Laser for *in-situ* NO Monitoring of Industrial Exhaust Systems, *Appl. Phys. B* 80, 617–625 (2005).

56. J. Faist, M. Beck, T. Aellen, and E. Gini, Quantum cascade laser based on bound-to-continuum transition, *Appl. Phys. Lett* 78, 147–149 (2001).

57. R. Maulini, A. Mohan, M. Giovannini, J. Faist, and E. Gini, External cavity quantum-cascade laser tunable from 8.2 to 10.4 μm using a gain element with a heterogeneous cascade, *Appl. Phys. Lett.* 88, 201113 (2006).

58. R. Maulini, D. A. Yarekha, J-M Bulliard, M. Giovannini, J. Faist, and E. Gini Continuous-wave operation of a broadly tunable thermoelectrically cooled external cavity quantum-cascade laser, *Opt. Lett* 30, 2584–2586 (2005).

59. G. R. Price, K. K. Botros, and G. M. Goldin, CFD Predictions and Field Measurements of NOx Emissions From LM1600 Gas Turbine During Part Load Operation, *Journal of Engineering for Gas Turbines and Power* 124, 276–283 (2002).

60. C. Stroud, S. Madronich, E. Atlas, B. Ridley, F. Flocke, A. Weinheimer, B. Talbot, A. Fried, B. Wert, R. Shetter, B. Lefer, M. Coffey, B. Heikes, and D. Blake, Photochemistry in the arctic free troposphere: NO_x budget and the role of odd nitrogen reservoir recycling, *Atmospheric Environment* 37, 3351–3364 (2003).

61. P. E. Silkoff, M. Caramori, L. Tremblay, P. McClean, C. Chaparro, S. Kesten, M. Hutcheon, A. S. Slutsky, N. Zamel, and S. Keshavjee, Exhaled Nitric Oxide In Human Lung Transplantation A Noninvasive Marker of Acute Rejection, *American Journal Of Respiratory and Critical Care Medicine* 157, 1822–1828 (1998).

62. S. A. Kharitonov and P. J. Barnes, Exhaled Markers of Pulmonary Disease, American Journal of Respiratory and Critical Care Medicine 163, 1693–1722 (2001).

63. K. Namjou, C. B. Roller, T. E. Reich, J. D. Jeffers, G. L. McMillen, P. J. McCann, M. A. Camp, Determination of exhaled nitric oxide distributions in a diverse sample population using tunable diode laser absorption spectroscopy *Appl. Phys. B* 85, 427–435 (2006).

64. J. B. McManus, D. D. Nelson, S. C. Herndon, J. H. Shorter, M. S. Zahniser, S. Blaser, L. Hvozdara, A. Muller, M. Giovannini, and J. Faist, Comparison of CW and Pulsed Operation with a TE-Cooled Quantum Cascade Infrared Laser for Detection of Nitric Oxide at 1900 cm-1, *Appl. Phys. B* 85, 235–241 (2006).

65. J. Ye, L.-S. Ma, and J. L. Hall, Sub-Doppler optical frequency reference at 1.064 μm by means of ultrasensitive cavity-enhanced frequency modulation spectroscopy of a C_2HD overtone transition, *Opt. Let.* 21, 1000–1002 (1996).

66. M. S. Taubman, D. C. Scott, T. L. Myers, and B. D. Cannon, Long wave infrared cavity enhanced sensors using quantum cascade lasers, Proc. of SPIE, 6010, 60100C-1 (2005).

67. B. A. Paldus, C. C. Harb, T. G. Spence, R. N. Zare, C. Gmachl, F. Capasso, D. L. Sivco, J. N. Baillargeon, A. L. Hutchinson, and A. Y. Cho, Cavity ringdown spectroscopy using mid-infrared quantum-cascade lasers, *Opt. Lett*., 25, 666–668, (2000).

68. G. von Basum, D. Halmer, P. Hering, M. Muertz, S. Schiller, F. Mueller, A. Popp, and F. Kuehnemann, Parts per trillion sensitivity for ethane in air with an optical parametric oscillator cavity leak-out spectrometer, *Opt. Lett*. 29, 797–799 (2004)

69. A. A Kosterev, A. A. Malinovsky, F. K. Tittel, C. Gmachl, F. Capasso, D. L. Sivco, J. N. Baillargeon, A. L. Hutchinson, and A. Y. Cho, Cavity ringdown spectroscopic detection of nitric oxide with a continuous-wave quantum-cascade laser, *Appl. Opt.* 40, 5522–5529, (2001).

70. M. L. Silva, D. M. Sonnenfroh, D. I. Rosen, M. G Allen, A. O'Keefe, Integrated cavity output spectroscopy measurements of nitric oxide levels in breath with a pulsed room – temperature quantum cascade laser, *Appl. Phys B* 81,705 (2005).

71. Y. A. Bakhirkin, A. A. Kosterev, R. Curl, F. K. Tittel, D. A. Yarekha, L. Hvozdara, M. Giovannini, and J. Faist, Sub-ppbv Nitric Oxide Concentration Measurements using CW Room-Temperature Quantum Cascade Laser based Integrated Cavity Spectroscopy, *Appl. Phys. B* 82, 149–154 (2006).

72. M. McCurdy, Y. Bakhirkin, and F. K. Tittel, "Quantum cascade laser-based integrated cavity output spectroscopy of exhaled nitric oxide", *Appl. Phys. B* **85,** 445–452 (2006).

73. D. D. Nelson, J. B. McManus, S. C. Herndon, J. Shorter, M. S. Zahniser, S. Blaser, L. Hvozdara, A. Mueller, M. Giovannini, and J.Faist, Spectral Characterization of a near-room temperature, continuous-wave quantum cascade laser for long-term, unattended monitoring of nitric oxide in the atmosphere, *Opt. Lett*. 21, 2012–2014 (2006).

74. J. H. Miller, Y. A. Bakhirkin, T. Ajtai, F. K. Tittel, C. J. Hill, and R. Q. Yang, Detection of formaldehyde using off-axis integrated cavity output spectroscopy with an interband cascade laser, *Appl. Phys B* 85, 391–396 (2006).

75. C. Gmachl, D. L. Sivco, R. Colombelli, F. Capasso, and A. Y. Cho, Ultra-broadband semiconductor laser, *Nature* 415, 883–887 (2002).